Masuda *et al.* isolated α-synuclein dimers formed in the presence of inhibitory compounds,[3] and the isolated soluble dimers were recently characterized using a panel of epitope-specific α-synuclein antibodies.[12] The reactivities of the antibodies indicated that the conformations of polyphenol-bound α-synuclein dimers differ from those of unbound monomers, but resemble those of amyloid fibrils, suggesting that inhibitor-bound molecular species are on-pathway intermediates.

This situation prompted us to carry out a comprehensive analysis of inhibitor-treated α-synucleins by means of NMR spectroscopy in conjunction with other biochemical methods, such as peptide mapping, immunoblotting, and redox-cycling staining. We have previously analyzed the antibody binding and site-specific phosphorylation of α-synuclein using ultra-high-field NMR spectroscopy.[13] For the structural characterization, we prepared and purified a ^{15}N-labeled α-synuclein dimer in the presence of polyphenol inhibitors on a milligram scale and analyzed it by ultra-high-field NMR spectroscopy recorded at a proton observation frequency of 920 MHz.

Results and Discussion

Isolation and characterization of inhibitor-bound α-synuclein dimer and monomer

SDS-stable, noncytotoxic α-synuclein oligomers were detected in the soluble fraction in the presence of inhibitory compounds such as polyphenols.[3] For detailed characterization of inhibitor-induced α-synuclein oligomers, we attempted to prepare exifone-, gossypetin-, and dopamine-induced α-synuclein dimer and monomer (for inhibitor structures, see Fig. 1) and to separate them by gel-filtration chromatography as described.[12] Fig. 2a shows the HPLC patterns of control and exifone-treated α-synucleins. The HPLC fractions of exifone-treated α-synuclein were analyzed by SDS-PAGE and Western blotting (Fig. 2b). The data indicate that the exifone-treated α-synuclein dimer (Exi-dimer) was successfully purified by gel-filtration chromatography. The homogeneity of inhibitor-induced monomer and dimer was also checked by diffusion NMR experiments (data not shown). α-Synuclein monomer and dimer treated with exifone, as well as control monomer (without inhibitor), were subjected to matrix-assisted laser desorption/ionization time-of-flight (MALDI-TOF) MS measurements (Fig. 2c). α-Synuclein monomer (control) showed a major signal at 14,460 Da, which matched the predicted mass (14,460 Da). On the other hand, exifone-treated monomer (Exi-monomer) gave a major signal at 14,524 Da, which corresponded to that of α-synuclein plus 64 Da. Exifone-bound α-synuclein (molecular mass of exifone, 278.2 Da) was not detected, presumably because exifone binding was noncovalent. The MS spectrum of Exi-dimer showed a broad peak at around 30 kDa and 15 kDa, and we could not obtain an accurate molecular mass. The peak at 15 kDa might be the doubly charged ion of the Exi-dimer and/or the monomer released from the Exi-dimer in the ionization process. To estimate the ratio of exifone bound to α-synuclein dimer and monomer, absorption of exifone at 385 nm was measured for Exi-dimer and Exi-monomer. The results indicate that Exi-dimer contains around 3

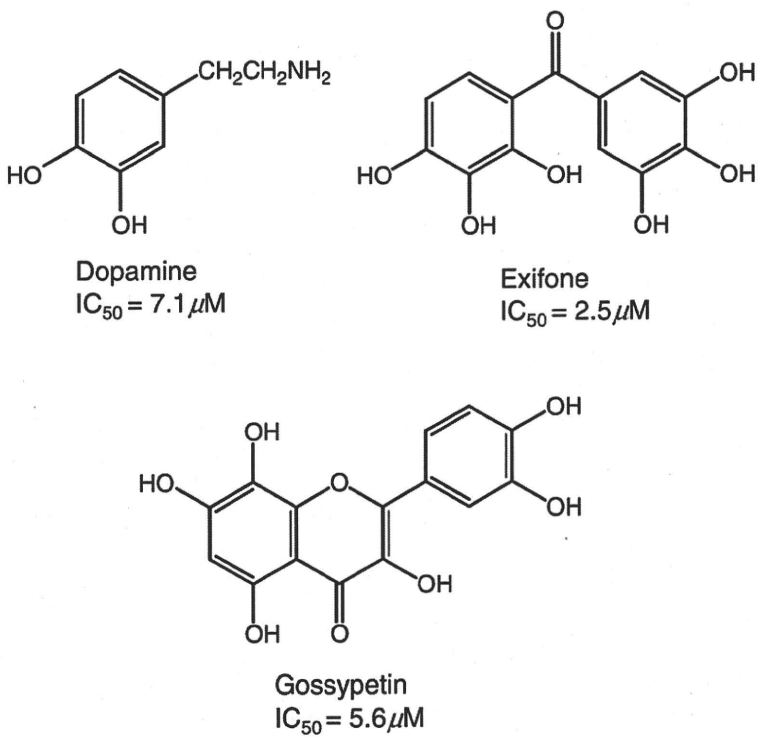

Fig. 1. Chemical structures of dopamine, exifone, and gossypetin with their IC_{50} values for inhibition of α-synuclein filament assembly.[3]

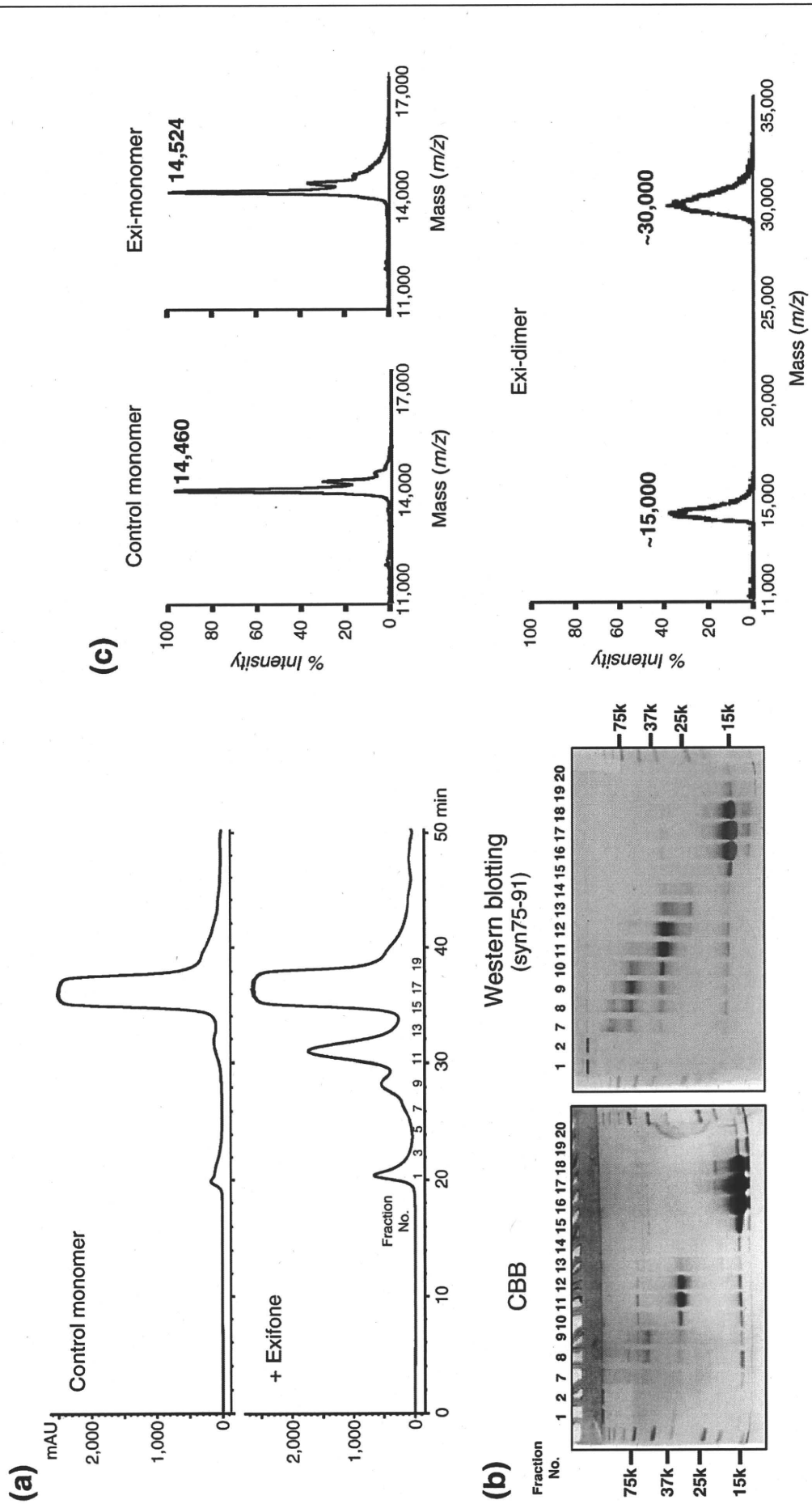

Fig. 2. Isolation and characterization of exifone-bound α-synucleins. (a) Separation of exifone-treated α-synuclein monomer and dimer by gel-filtration chromatography (detection: absorbance at 214 nm). (b) SDS-PAGE of fractions separated by gel-filtration chromatography (Coomassie brilliant blue staining and Western blotting). Pooled fractions 11–12 and 16–18 were used as Exi-dimer and Exi-monomer, respectively. (c) Partial MALDI-TOF MS spectra of α-synuclein monomer (control), Exi-monomer, and Exi-dimer.

molecules of exifone per α-synuclein monomer, while Exi-monomer contains one exifone molecule per α-synuclein chain (Supplementary Fig. S1).

For the identification of the modification (corresponding to a molecular mass of 64 Da) found in the Exi-monomer, α-synuclein was incubated with various concentrations of exifone (0, 0.2, 0.5, 1, and 2 mM) and the resulting samples were analyzed by MS (Supplementary Fig. S2). The molecular mass of α-synuclein increased in an exifone concentration-dependent manner and reached 14,528 Da (Supplementary Fig. S2a and b). A similar increase in molecular mass was reported in the presence of H_2O_2, which oxidized methionine residues to methionine sulfoxide.[14] Methionine oxidation is known to increase mass by 16 Da. α-Synuclein has four methionine residues, Met1, Met5, Met116, and Met127, and thus the oxidation of all the methionine residues would result in an increase in mass of 64 Da (Supplementary Fig. S3c). Indeed, α-synuclein incubated with various concentrations of H_2O_2 showed a concentration-dependent increase in molecular mass of up to 14,533 Da (Supplementary Fig. S3a and b), similar to that seen in the case of exifone. These results strongly suggest that all the methionine residues of Exi-monomer were oxidized to methionine sulfoxide.

Peptide mapping of inhibitor-induced α-synuclein dimer and monomer

In order to confirm the oxidation of methionine, control α-synuclein, Exi-monomer, Exi-dimer, and H_2O_2-treated α-synuclein monomer were digested with trypsin, and the resulting peptide mixtures were analyzed by reverse-phase HPLC (Fig. 3a). The elution patterns of peptides derived from Exi-monomer and Exi-dimer exhibited different profiles compared with that of control α-synuclein. Peaks 5 and 10 in the map of control α-synuclein were absent in the maps of Exi-monomer and Exi-dimer. Instead, peaks 11–18 newly appeared in the maps of Exi-monomer and Exi-dimer. The patterns of Exi-monomer and Exi-dimer were similar to those of α-synuclein oxidized with H_2O_2. All the peaks were analyzed by MS and the results are summarized in Fig. 3b. Peaks 5 and 10 were identified as Met1–Lys6 (containing two methionines, Met1 and Met5) and Asn103–Ala140 (containing Met116 and Met127), respectively. In the case of Exi-monomer or Exi-dimer, peaks 11, 15, and 19 were identified as Met1–Lys6 including two oxidized methionines. Peaks 12, 16, and 20 were identified as Asn103–Ala140 including oxidized Met116 and Met127. Peaks 13, 14, 16, and 17 were derived from Asn103–Ala140 oxidized at either Met116 or Met127. Similar results were obtained for dopamine-bound dimer and monomer (data not shown). These results clearly indicate that the inhibitors exifone and dopamine have the ability to oxidize methionine residues on α-synuclein. It is established that α-synuclein assembly was inhibited by exifone at low micromolar range (IC_{50}=2.5 μM),[3] and methionine sulfoxide could not be detected at a low concentration of exifone (data not shown). These findings suggest that the stabilization of intermediate oligomers by small molecules is responsible for the inhibition of filament formation, and oxidation of methionine does not seem to play a major role in inhibition.

No covalent inhibitor–peptide adducts or cross-linked peptides were detected in the peptide mapping experiments, indicating that the inhibitors bind noncovalently to α-synuclein and that α-synuclein dimer is formed in a noncovalent fashion. These observations are consistent with the results of MALDI MS analysis of Exi-monomer, which showed no inhibitor adducts (Fig. 2c). Our extensive liquid chromatography–electrospray ionization MS analysis also did not show the covalent inhibitor adducts or α-synuclein dimer (data not shown). Further, more detailed biochemical studies to investigate the modes of inhibitor binding and dimerization are currently in progress.

Characterization of exifone-binding regions in α-synuclein

Exifone is an antioxidant and thus can be detected by redox-cycling staining, which is a well-established method for detecting quinoproteins.[15] As expected, Exi-dimer and Exi-monomer were stained as purple bands by redox-cycling staining due to nitroblue tetrazolium (NBT) reduction to formazan (Fig. 4a), while untreated control α-synuclein showed no staining. This result shows that redox-cycling staining is useful for examining the exifone-binding regions in α-synuclein. In order to determine the binding region of exifone and the regions involved in the dimerization, Exi-dimer was digested with endoproteinase Asp-N and the resulting peptides were detected with silver or redox-cycling staining. Asp-N digestion of Exi-dimer gave two major fragments, corresponding to molecular masses of 20 kDa (no. 1) and 16 kDa (no. 2), on SDS-PAGE after silver staining (Fig. 4b). These two bands were positive for redox-cycling staining. Since α-synuclein monomer migrates at 15 kDa, these fragments represent dimeric peptides stabilized by exifone. α-Synuclein has six aspartic acid residues (Asp2, Asp98, Asp115, Asp119, Asp121, and Asp135). Immunoblot analysis with a panel of site-specific anti-α-synuclein antibodies (Fig. 5) suggested that the 20-kDa fragment contains the dimerized N-terminal fragment Met1–Met97 of α-synuclein (cleaved at the N-terminus of Asp98). The 16-kDa fragment was also labeled with antibodies to the N-terminal and central portions of α-synuclein (residues 1–50). It has been reported that Asp-N cleaves peptide bonds N-terminal to glutamate as well as aspartate residues.[16,17] Glu57 and/or Glu61 are found in the middle of α-synuclein and are candidate Asp-N cleavage sites to produce the 16-kDa fragment. The reactivity of anti-α-synuclein antibodies and the relaxed specificity of Asp-N indicate that the 16-kDa fragment corresponds to a dimer composed of Met1–Ala56/Lys60. These results suggest that the N-

terminal region (1–60) of α-synuclein is involved in the dimerization and exifone binding. This is in contrast with a previous report by Norris *et al.*, in which they suggested that dopamine inhibited the aggregation of α-synuclein by binding to the C-terminal residues 125–129 (i.e., YEMPS) and stabilizing the soluble oligomers.[6] The discrepancy might be due to the fact that they analyzed the dopamine-binding sites by using deletion mutants lacking the C-terminal regions and did not use full-length α-synucleins.

High-resolution NMR spectra of inhibitor-bound α-synuclein monomer and dimer

In order to characterize the behavior of α-synuclein monomer and dimer formed in the presence of polyphenolic compounds, we conducted a structural analysis of inhibitor-bound α-synuclein monomer and dimer using ultra-high-field NMR spectroscopy. NMR signals of backbone amides constitute excellent probes to provide maps of the interacting sites and to examine the effects of modifications.[13] Fig. 6a and b shows the ^{1}H–^{15}N heteronuclear single quantum coherence (HSQC) spectra of uniformly ^{15}N-labeled Exi-monomer and Exi-dimer, as well as control monomer, recorded at a proton observation frequency of 920 MHz. The amide resonances of Exi-monomer and Exi-dimer were assigned by comparing the NMR spectral data with those of control α-synuclein monomer. Little chemical shift difference was detected between Exi-monomer and control monomer for most observed peaks, except for the signals corresponding

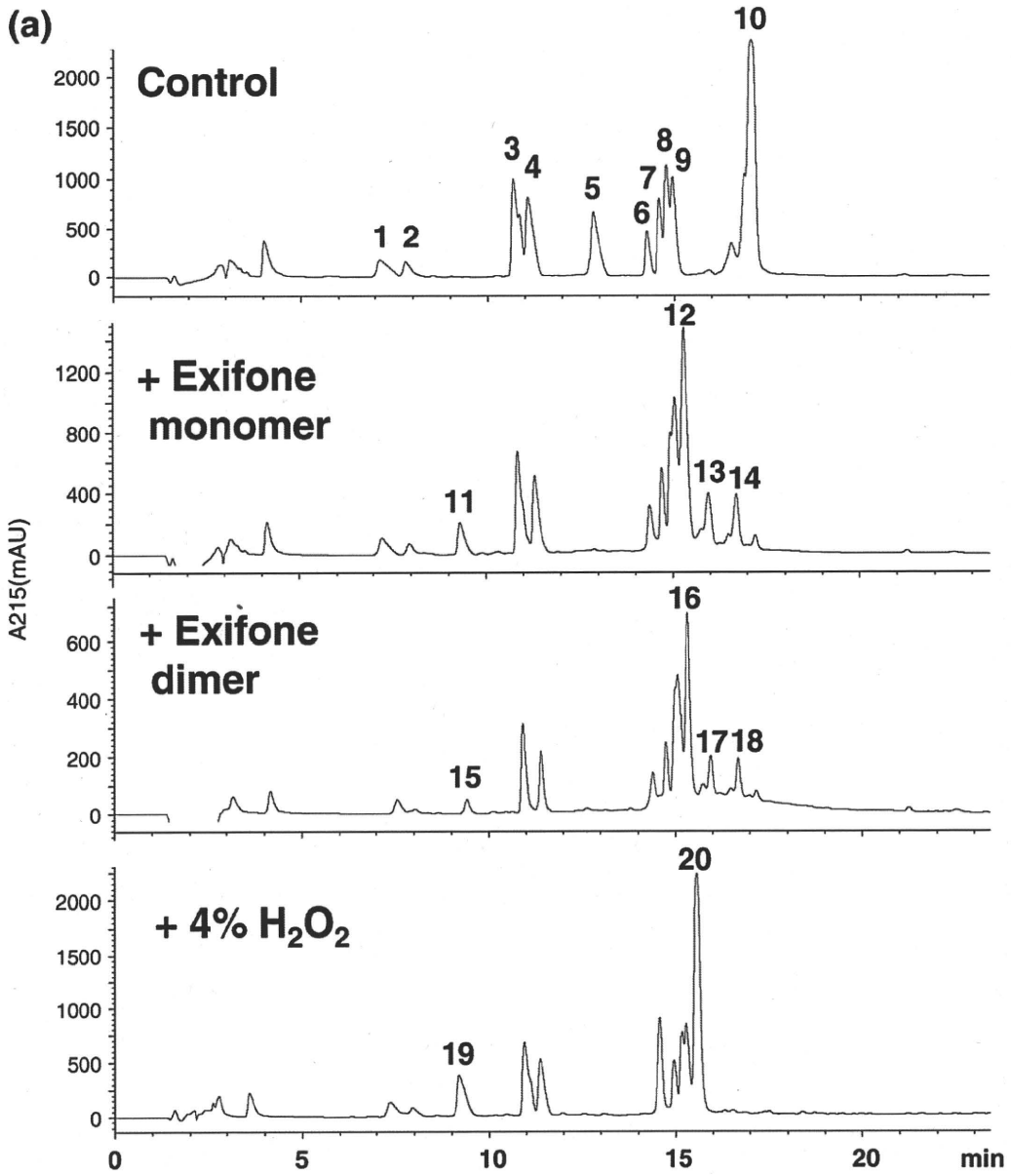

Fig. 3. Tryptic peptide mapping and MS analysis of α-synucleins. (a) Reverse-phase HPLC patterns of monomeric α-synuclein (control), Exi-monomer, Exi-dimer, and H_2O_2-treated α-synuclein monomer. (b) Observed masses and peak assignments of the peptides separated on a reverse-phase column. Oxidation of methionine residues was observed in Exi-monomer and Exi-dimer, as well as H_2O_2-treated α-synuclein monomer.

(b)

Peak No.	$(M+H)^+$ Observed	$(M+H)^+$ Calculated	Assignment
1	830.6 873.5 1072.6	830.4 873.4 1072.5	QGVAEAAGK (24-32) EGVVAAAEK (13-21) AKEGVVAAAEK (11-21)
2	1180.7 1295.8 1524.8	1180.6 1295.6 1524.8	TKEGVLYVGSK (33-43) EGVVHGVATVAEK (46-58) TKEGVVHGVATVAEK (44-58)
3	951.5	951.5	EGVLYVGSK (35-43)
4	1295.7	1295.6	EGVVHGVATVAEK (46-58)
5	770.5	770.3	MDVFMK (1-6)
6	1606.6	1606.8	TVEGAGSIAAATGFVKK (81-97)
7	2157.2	2157.1	TKEQVTNVGGAVVTGVTAVAQK (58-80)
8	1478.5	1478.7	TVEGAGSIAAATGFVK (81-96)
9	1928.0	1928.0	EQVTNVGGAVVTGVTAVAQK (61-80)
10	4295.0	4286.7	NEEGAPQEGILEDMPVDPDNAYEMPSEEGYQDYEPEA (103-140)
11	803.0	802.3.0	M*DVFM*K (1-6) (M*:methionine sulfoxide)
12	4322.0	4318.7	NEEGAPQEGILEDM*PVDPDNAYEM*PSEEGYQDYEPEA (103-140)
13	4311.0	4302.7	NEEGAPQEGILEDM#PVDPDNAYEM#PSEEGYQDYEPEA (103-140) (One of two methionine residues (M#) was oxidized)
14	4312.0	4302.7	NEEGAPQEGILEDM#PVDPDNAYEM#PSEEGYQDYEPEA (103-140)
15	802.0	802.3	M*DVFM*K (1-6)
16	4322.0	4318.7	NEEGAPQEGILEDM*PVDPDNAYEM*PSEEGYQDYEPEA (103-140)
17	4311.0	4302.7	NEEGAPQEGILEDM#PVDPDNAYEM#PSEEGYQDYEPEA (103-140)
18	4312.0	4302.7	NEEGAPQEGILEDM#PVDPDNAYEM#PSEEGYQDYEPEA (103-140)
19	803.0	802.3	M*DVFM*K (1-6)
20	4322.0	4318.7	NEEGAPQEGILEDM*PVDPDNAYEM*PSEEGYQDYEPEA (103-140)

Fig. 3 *(legend on previous page)*

to Met5, Met116, Met127, and their neighboring residues (Fig 6a). The observed chemical shift differences are mostly attributable to the oxidation of methionine residues. The differences in peak intensities between Exi-monomer and control monomer were also generally small (Fig. 6c). These results indicate that the dynamical features of both synuclein monomers are almost the same, and methionine oxidation itself does not greatly influence the structural characteristics of α-synuclein.

It is noteworthy that significant reductions in signal intensity [I(Exi-dimer)/I(control monomer)< 0.8] were observed for the peaks originating from the N-terminal region (1–60) of Exi-dimer compared with the control monomer (Fig. 6d). This result shows that the N-terminal regions are involved in exifone-induced dimerization of α-synuclein, in accordance with the results obtained from Asp-N digestion of the Exi-dimer. The gradual reduction in the signal intensities might be explained by heterogeneous dimerization around the N-terminus. The observed reduction in signal intensity, in our case, was not due to chemical exchange between the inhibitor-free and inhibitor-bound states of α-synuclein, as had been suggested by Rao *et al.*,[10] because the inhibitor-induced dimer and monomer were each purified to homogeneity and free or exchangeable inhibitors were removed by gel-filtration column chromatography and buffer exchange. Similar NMR spectra were observed for dopamine- and gossypetin-induced dimers (Supplementary Fig. S4), indicating that the N-terminal dimerization modes induced by dopamine, exifone, and gossypetin are the same or at least very similar. On the other hand, the C-terminal portion of exifone-bound dimer was still predominantly random coil in character, as observed in the control monomeric α-synuclein. These

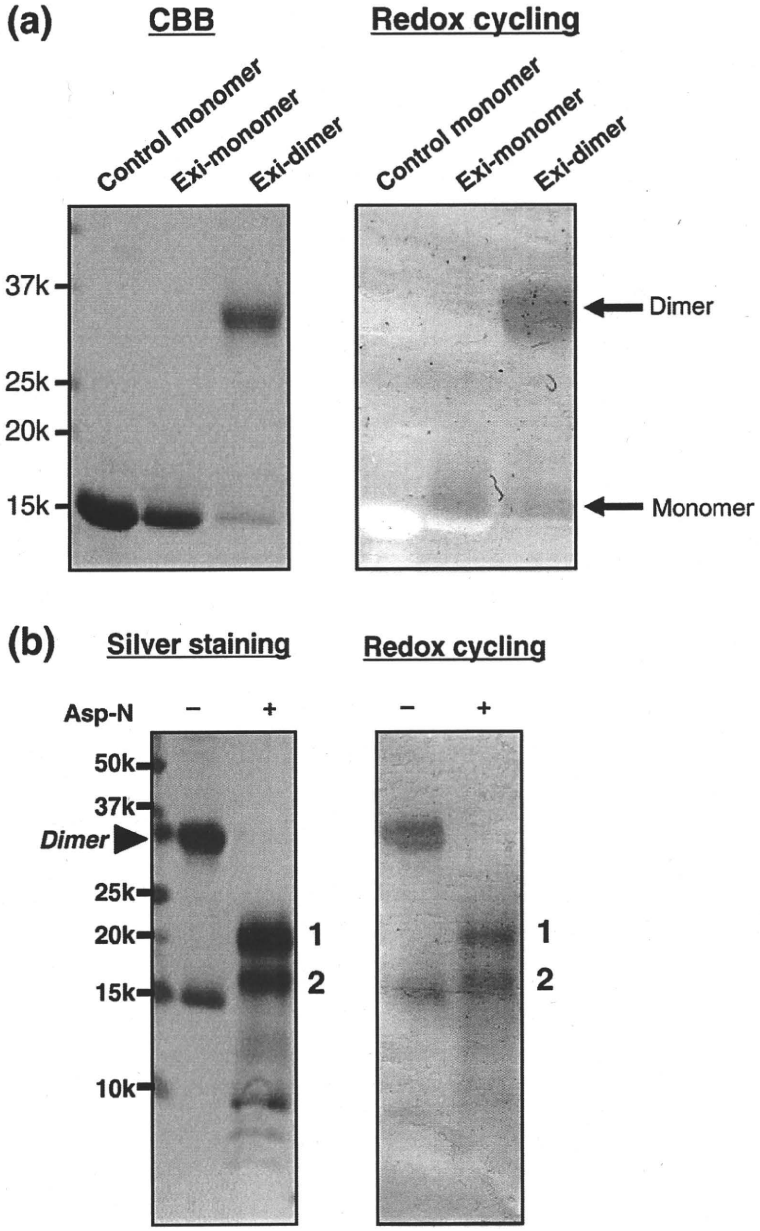

Fig. 4. Detection of exifone bound to α-synucleins by redox-cycling staining. (a) Control monomer, Exi-monomer, and Exi-dimer were stained with Coomassie brilliant blue (left) or by redox cycling (right). Exifone-bound α-synucleins were stained by redox cycling, appearing as purple-blue bands in the Exi-monomer and Exi-dimer lanes, due to NBT reduction to formazan (right). (b) Asp-N digestion of Exi-dimer. Exi-dimer was digested with endoproteinase Asp-N and the fragments were detected by silver staining (left) and redox staining (right). Two major bands corresponding to 20 kDa and 16 kDa (nos. 1 and 2, respectively) were positive for redox-cycling staining.

observations indicate the importance of the N-terminal region in α-synuclein assembly.

It is of note that three missense mutations in familial PD (A30P, E46K, and A53T) are located in the N-terminal region of α-synuclein. Recent NMR analyses suggest that these mutations may be altering the physicochemical properties of the protein, such as net charge (E46K) and secondary-structure propensity (A30P and A53T).[19] The binding of exifone, gossypetin, or dopamine to α-synuclein might also alter the net charge and/or secondary-structure propensity.

We did not observe the colloidal formation of exifone, gossypetin, or dopamine by electron microscopy (data not shown) as reported by Feng *et al.*[5] The discrepancy might be due to differences in the compounds used or differences in the proteins investigated. The inhibition mechanism of these three compounds seems rather specific because the N-terminal region was specifically involved in inhibitor binding, which is in contrast to the nonspecific colloidal inhibition.

In summary, we have characterized the inhibitor-bound α-synuclein dimer and showed that the N-terminal region (1–60) plays a key role in dimerization and inhibitor binding. Further studies are under way in our laboratory to elucidate the mechanisms of inhibitor-induced oligomer formation at atomic resolution.

Materials and Methods

Antibodies

Polyclonal antibodies were raised against synthetic peptides corresponding to residues 1–10, 11–20, 21–30, 31–40, 41–50, 51–60, 61–70, 75–91, and 131–140 of human α-synucleins, prepared as described previously.[12] Antibody

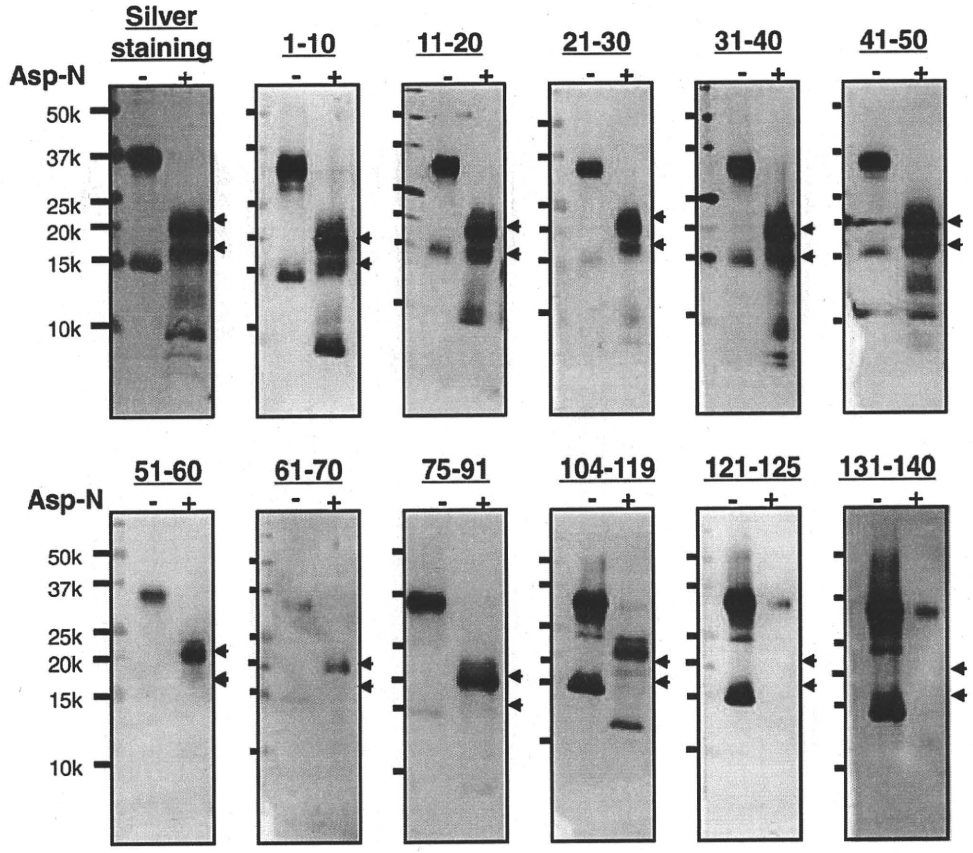

Fig. 5. Immunoblot analysis of Asp-N digests of Exi-dimer. Silver staining and immunoblots of Asp-N digests of Exi-dimer with a panel of anti-α-synuclein antibodies raised against nine peptides (corresponding to residues 1–10, 11–20, 21–30, 31–40, 41–50, 51–60, 61–70, 75–91, and 131–140).[12] Experimental details are given in Materials and Methods. Two major fragments (band nos. 1 and 2) were detected with silver staining (indicated with arrowheads). Fragment no. 1 was positive for antibodies to the N-terminal region, 1–97, and no. 2 was positive for antibodies to the N-terminal region, 1–50.

Syn259, which recognizes residues 104–119 of α-synuclein, was kindly provided by Dr. S. Nakajo. Monoclonal antibody Syn211, which recognizes residues 121–125 of α-synuclein, was purchased from Zymed.

Protein expression and purification

Expression of isotopically labeled α-synuclein was performed as described.[13] Human α-synuclein cDNA in bacterial expression plasmid pRK172 was used for production of isotopically labeled protein for NMR analyses.[20] Codon 136 was changed from TAC to TAT by site-directed mutagenesis to avoid cysteine misincorporation.[21] Uniformly ^{15}N-labeled α-synuclein was expressed in *Escherichia coli* BL21(DE3) cells grown in M9 minimal medium containing 1 g/L [^{15}N]NH_4Cl, while unlabeled α-synuclein was expressed using LB medium. Cell lysates were subjected to boiling and subsequently to ammonium sulfate precipitation. The precipitated α-synuclein was extensively dialyzed against 20 mM Tris–HCl (pH 8.0) and then purified with DEAE ion-exchange chromatography.

Preparation of inhibitor-bound α-synuclein monomers and dimers

Purified ^{15}N-labeled recombinant α-synuclein (9 mg/mL) was incubated with 2 mM inhibitor (exifone, gossypetin, or dopamine; see Fig. 1) for 30 days at 37 °C in 30 mM Tris–HCl containing 0.1% sodium azide. The samples were then centrifuged at 113,000*g* for 20 min. The supernatants were loaded on a Sephadex G-25 gel-filtration column to separate oligomers from unbound inhibitor. The eluates were fractionated on a Superdex 200 gel-filtration column (1 cm×30 cm), eluted with 10 mM Tris–HCl (pH 7.5) containing 150 mM NaCl. Eluates were monitored at 215 nm. α-Synuclein monomer and dimer fractions were each concentrated and the concentrates were subjected to NMR analysis. Protein concentrations were determined using HPLC and bicinchoninic acid protein assay kit (Pierce).

Mass spectrometry

Samples were spotted on a sample plate and mixed with the matrix solutions, saturated sinapic acid (Fluka) or α-cyano-4-hydroxycinnamic acid (Fluka) in 50% acetonitrile/H_2O containing 0.1% (v/v) trifluoroacetic acid. Mass spectra were obtained by MALDI-TOF MS using a Voyager-DE Pro mass spectrometer (PerSeptive Biosystems).

Peptide mapping of H_2O_2-treated and inhibitor-bound α-synucleins

Inhibitor-bound α-synuclein monomer and dimer were prepared as described above. For methionine oxidation, α-synuclein monomer (7 mg/mL) was incubated with 0–4% H_2O_2 at room temperature for 20 min and then dialyzed

against 30 mM Tris–HCl (pH 7.5) to remove H_2O_2. To identify the modification, inhibitor-bound α-synuclein monomer and dimer, as well as H_2O_2-treated α-synuclein, were incubated with trypsin at 37 °C for 18 h at an enzyme-to-substrate ratio of 1:50 (mol/mol) in 30 mM Tris–HCl (pH 7.5). Digested peptide products were separated by reverse-phase HPLC on a Supersphere Select B column (2.1 × 125 mm; Merck) and analyzed by MALDI-TOF MS.

Determination of stoichiometry of exifone/α-synuclein complexes

The stoichiometry of exifone/α-synuclein complexes was determined by measuring the absorbance of exifone at 385 nm using a spectrophotometer (UV-1600 PC, Shimadzu Co). Exifone-bound monomeric and dimeric α-synucleins were isolated by gel-filtration chromatography as described above.

Redox-cycle staining

Samples were subjected to SDS-PAGE and transferred onto polyvinylidene fluoride membranes. The membranes were incubated in 0.24 mM NBT (Sigma), 2 M potassium glycinate solution (pH 10.0) in the dark for 16 h at room temperature and then dipped in 100 mM sodium borate (pH 10.0). Exifone-bound α-synuclein was specifically stained as purple-blue bands due to NBT reduction to formazan.

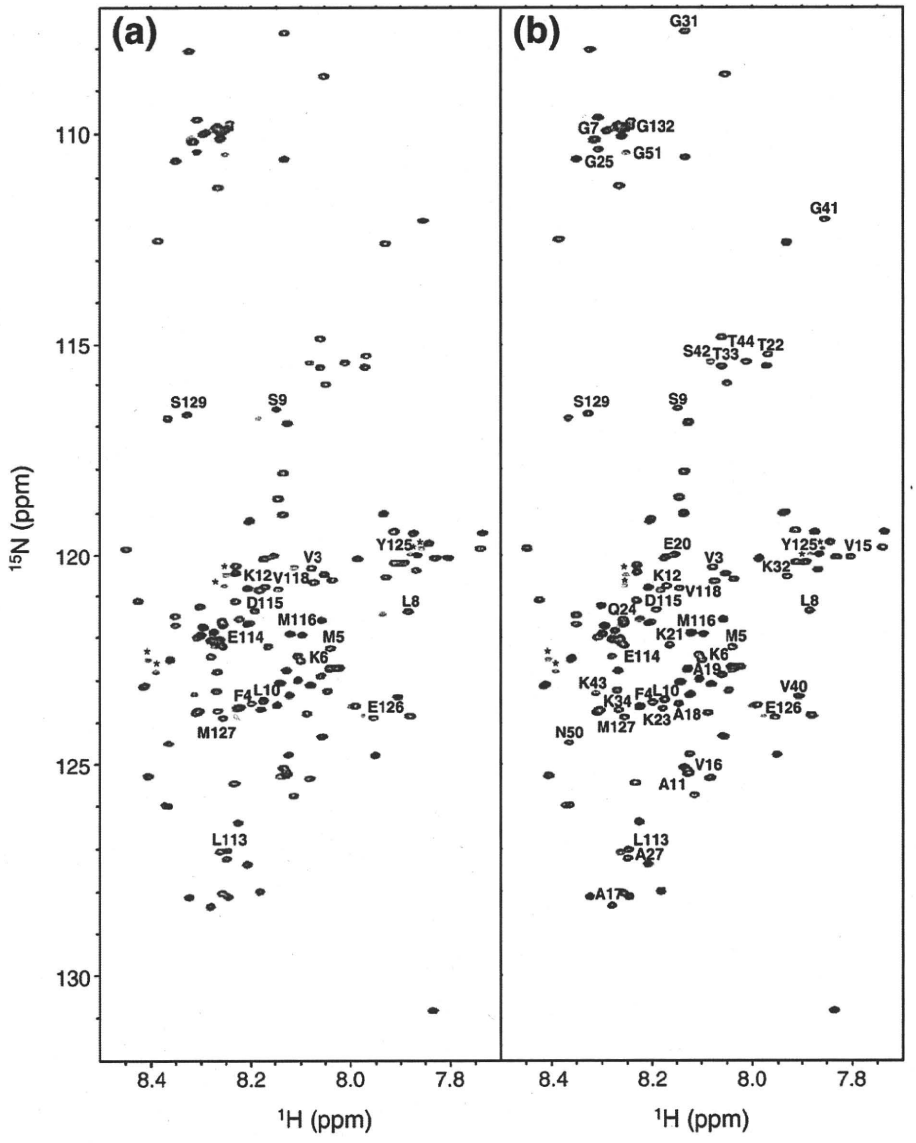

Fig. 6. NMR spectral comparison of exifone-bound ^{15}N-labeled α-synuclein dimer and control monomer. (a) ^{1}H–^{15}N HSQC spectra of ^{15}N-labeled Exi-monomer (red) and ^{15}N-labeled control monomer (black) recorded at a proton frequency of 920 MHz. (b) ^{1}H–^{15}N HSQC spectra of ^{15}N-labeled Exi-dimer (red) and ^{15}N-labeled control monomer (black). (c) Plot of the relative peak intensities, *I*(Exi-monomer)/*I*(monomer), of the HSQC cross-peaks in the Exi-monomer and control monomer *versus* the amino acid sequence of α-synuclein. (d) *I*(Exi-dimer)/*I*(monomer) of the HSQC cross-peaks in the Exi-dimer and control monomer. Signals derived from oxidized methionines and their neighboring residues (indicated with asterisks in a and b) were split and not taken into account. The peak splittings mostly reflect a mixture of *R* and *S* isomers of methionine sulfoxide.[18]

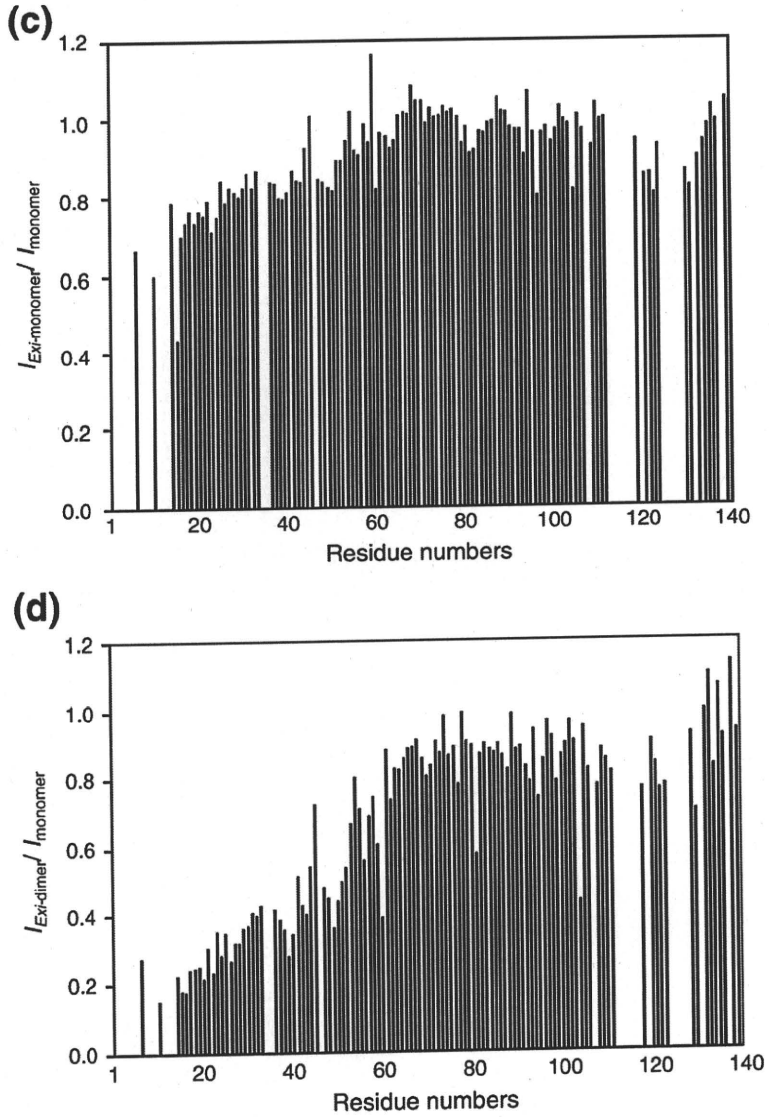

Fig. 6 *(legend on previous page)*

Asp-N digestion of α-synuclein dimer

α-Synuclein dimer (0.25 mg/mL) in 30 mM Tris–HCl (pH 7.5) was treated with 40 μg/mL of Asp-N (Roche) at 37 °C for 1 h. The reaction was stopped by adding 2× SDS sample buffer [4% SDS, 0.16 M Tris–HCl (pH 6.8), 30% glycerol] and the solution was boiled for 5 min. The samples were loaded onto 15% Tris/tricine SDS-PAGE gel, and the digested products were detected by silver staining (kit from Wako), immunoblotting, and redox-cycling staining. For immunoblotting, SDS-PAGE gels were blotted onto polyvinylidene fluoride membranes, blocked with 3% gelatin/phosphate-buffered saline, and incubated overnight at room temperature with anti-α-synuclein antibody in 10% FBS/phosphate-buffered saline. After washing, the blots were incubated for 2 h at room temperature with biotinylated secondary antibody (1:500) (Vector Laboratories). Following further washing, the blots were incubated with peroxidase-labeled avidin–biotin (Vector laboratories) for 30 min at room temperature and developed with $NiCl_2$-enhanced diaminobenzidine (Sigma).

NMR measurements

The samples for NMR experiments were prepared at a concentration of 0.1–1.0 mM in 90% H_2O/10% D_2O (v/v), 10 mM sodium phosphate buffer, and 100 mM NaCl at pH 7.0. NMR experiments were performed at 10 °C using a JEOL JNM-ECA920 spectrometer equipped with a 5-mm triple resonance probe. Backbone assignments of α-synuclein monomer were achieved by means of standard triple resonance experiments, as described previously.[13] The samples were checked by SDS-PAGE before and after NMR measurements, and it was confirmed that aggregation of inhibitor-bound α-synuclein monomer and dimer did not occur under these conditions. NMR time domain data were processed with the nmrPipe package[22] and the spectra were analyzed by using

Sparky software (T. D. Goddard and D. G. Kneller, University of California, San Francisco).

Acknowledgements

We thank K. Senda and K. Hattori (Nagoya City University) for help in the preparation of the recombinant proteins for NMR spectroscopy. We also thank M. Nakano (IMS) and T. Sugihara (JEOL) for help in NMR measurements and K. Matsumoto (RIKEN) for assistance in MS. We thank Drs. H. Sezaki, A. Hayashi, and T. Hosono (Agilent Technologies Japan) for their kind support in liquid chromatography–electrospray ionization MS analysis. This work was supported in part by Grants-in-Aid for Scientific Research on Priority Areas, Research on Pathomechanisms of Brain Disorders (to Y.Y., K.K., and M.H.), Grants-in-Aid for Scientific Research on Innovative Areas, Molecular Science of Fluctuations toward Biological Functions (to K.K.), and "Nanotechnology Network Project" of the Ministry of Education, Culture, Sports, Science and Technology (MEXT). This work was also supported by Takeda Science Foundation (Y.Y.).

Supplementary Data

Supplementary data associated with this article can be found, in the online version, at doi:10.1016/j.jmb.2009.10.068

References

1. Conway, K. A., Rochet, J. C., Bieganski, R. M. & Lansbury, P. T., Jr (2001). Kinetic stabilization of the α-synuclein protofibril by a dopamine-α-synuclein adduct. *Science*, **294**, 1346–1349.
2. Li, H. T., Lin, D. H., Luo, X. Y., Zhang, F., Ji, L. N., Du, H. N. *et al.* (2005). Inhibition of α-synuclein fibrillization by dopamine analogs via reaction with the amino groups of α-synuclein. Implication for dopaminergic neurodegeneration. *FEBS J.* **272**, 3661–3672.
3. Masuda, M., Suzuki, N., Taniguchi, S., Oikawa, T., Nonaka, T., Iwatsubo, T. *et al.* (2006). Small molecule inhibitors of α-synuclein filament assembly. *Biochemistry*, **45**, 6085–6094.
4. Porat, Y., Abramowitz, A. & Gazit, E. (2006). Inhibition of amyloid fibril formation by polyphenols: structural similarity and aromatic interactions as a common inhibition mechanism. *Chem. Biol. Drug Des.* **67**, 27–37.
5. Feng, B. Y., Toyama, B. H., Wille, H., Colby, D. W., Collins, S. R., May, B. C. *et al.* (2008). Small-molecule aggregates inhibit amyloid polymerization. *Nat. Chem. Biol.* **4**, 197–199.
6. Norris, E. H., Giasson, B. I., Hodara, R., Xu, S., Trojanowski, J. Q., Ischiropoulos, H. & Lee, V. M. (2005). Reversible inhibition of α-synuclein fibrillization by dopaminochrome-mediated conformational alterations. *J. Biol. Chem.* **280**, 21212–21219.
7. Herrera, F. E., Chesi, A., Paleologou, K. E., Schmid, A., Munoz, A., Vendruscolo, M. *et al.* (2008). Inhibition of α-synuclein fibrillization by dopamine is mediated by interactions with five C-terminal residues and with E83 in the NAC region. *PLoS ONE*, **e3394**, 3.
8. Ehrnhoefer, D. E., Bieschke, J., Boeddrich, A., Herbst, M., Masino, L., Lurz, R. *et al.* (2008). EGCG redirects amyloidogenic polypeptides into unstructured, off-pathway oligomers. *Nat. Struct. Mol. Biol.* **15**, 558–566.
9. Moussa, C. E., Mahmoodian, F., Tomita, Y. & Sidhu, A. (2008). Dopamine differentially induces aggregation of A53T mutant and wild type α-synuclein: insights into the protein chemistry of Parkinson's disease. *Biochem. Biophys. Res. Commun.* **365**, 833–839.
10. Rao, J. N., Dua, V. & Ulmer, T. S. (2008). Characterization of α-synuclein interactions with selected aggregation-inhibiting small molecules. *Biochemistry*, **47**, 4651–4656.
11. Hong, D. P., Fink, A. L. & Uversky, V. N. (2008). Structural characteristics of α-synuclein oligomers stabilized by the flavonoid baicalein. *J. Mol. Biol.* **383**, 214–223.
12. Masuda, M., Hasegawa, M., Nonaka, T., Oikawa, T., Yonetani, M., Yamaguchi, Y. *et al.* (2009). Inhibition of α-synuclein fibril assembly by small molecules: analysis using epitope-specific antibodies. *FEBS Lett.* **583**, 787–791.
13. Sasakawa, H., Sakata, E., Yamaguchi, Y., Masuda, M., Mori, T., Kurimoto, E. *et al.* (2007). Ultra-high field NMR studies of antibody binding and site-specific phosphorylation of α-synuclein. *Biochem. Biophys. Res. Commun.* **363**, 795–799.
14. Uversky, V. N., Yamin, G., Souillac, P. O., Goers, J., Glaser, C. B. & Fink, A. L. (2002). Methionine oxidation inhibits fibrillation of human α-synuclein *in vitro*. *FEBS Lett.* **517**, 239–244.
15. Paz, M. A., Gallop, P. M., Torrelio, B. M. & Fluckiger, R. (1988). The amplified detection of free and bound methoxatin (PQQ) with nitroblue tetrazolium redox reactions: insights into the PQQ-locus. *Biochem. Biophys. Res. Commun.* **154**, 1330–1337.
16. Ingrosso, D., Fowler, A. V., Bleibaum, J. & Clarke, S. (1989). Specificity of endoproteinase Asp-N (Pseudomonas fragi): cleavage at glutamyl residues in two proteins. *Biochem. Biophys. Res. Commun.* **162**, 1528–1534.
17. Tetaz, T., Morrison, J. R., Andreou, J. & Fidge, N. H. (1990). Relaxed specificity of endoproteinase Asp-N: this enzyme cleaves at peptide bonds N-terminal to glutamate as well as aspartate and cysteic acid residues. *Biochem. Int.* **22**, 561–566.
18. Stadtman, E. R., Van Remmen, H., Richardson, A., Wehr, N. B. & Levine, R. L. (2005). Methionine oxidation and aging. *Biochim. Biophys. Acta*, **1703**, 135–140.
19. Rospigliosi, C. C., McClendon, S., Schmid, A. W., Ramlall, T. F., Barre, P., Lashuel, H. A. & Eliezer, D. (2009). E46K Parkinson's-linked mutation enhances C-terminal-to-N-terminal contacts in α-synuclein. *J. Mol. Biol.* **388**, 1022–1032.
20. Jakes, R., Spillantini, M. G. & Goedert, M. (1994). Identification of two distinct synucleins from human brain. *FEBS Lett.* **345**, 27–32.
21. Masuda, M., Dohmae, N., Nonaka, T., Oikawa, T., Hisanaga, S., Goedert, M. & Hasegawa, M. (2006). Cysteine misincorporation in bacterially expressed human α-synuclein. *FEBS Lett.* **580**, 1775–1779.
22. Delaglio, F., Grzesiek, S., Vuister, G. W., Zhu, G., Pfeifer, J. & Bax, A. (1995). NMRPipe: a multidimensional spectral processing system based on UNIX pipes. *J. Biomol. NMR*, **6**, 277–293.

Acta Neuropathol (2010) 120:55–66
DOI 10.1007/s00401-010-0702-1

ORIGINAL PAPER

Phosphorylated TDP-43 pathology and hippocampal sclerosis in progressive supranuclear palsy

Osamu Yokota · Yvonne Davidson · Eileen H. Bigio · Hideki Ishizu · Seishi Terada · Tetsuaki Arai · Masato Hasegawa · Haruhiko Akiyama · Stephen Sikkink · Stuart Pickering-Brown · David M. A. Mann

Received: 15 March 2010 / Revised: 20 May 2010 / Accepted: 21 May 2010 / Published online: 30 May 2010

Abstract TDP-43 is characteristically accumulated in TDP-43 proteinopathies such as frontotemporal lobar degeneration and motor neurone disease, but is also present in some tauopathies, including Alzheimer's disease, argyrophilic grain disease, and corticobasal degeneration (CBD). However, several studies have suggested that cases of progressive supranuclear palsy (PSP) lack TDP-43 pathology. We have therefore examined limbic regions of the brain in 19 PSP cases, as well as in 12 CBD cases, using phosphorylation-dependent anti-TDP-43 antibodies. We observed TDP-43-positive inclusions in five PSP cases (26%), as well as in two CBD cases (17%). The amygdala and hippocampal dentate gyrus were most frequently affected in PSP. Regional tau burden tended to be higher in TDP-43-positive PSP cases, and a significant correlation between tau and TDP-43 burden was noted in the occipitotemporal gyrus. Hippocampal sclerosis (HS) was found in 3/5 TDP-43-positive PSP cases, but HS was significantly more frequent in TDP-43-positive than TDP-43 negative PSP cases. Dementia was present in 13/19 (58%) of the PSP cases, in 4/5 TDP-43-positive cases, in all 3 TDP-43-positive cases with HS, in 1/2 TDP-43-positive cases without HS, and 7/14 cases lacking both. TDP-43 and tau were frequently colocalized in the amygdala, but not in the hippocampal dentate gyrus. Immunoblotting demonstrated the characteristic (for TDP-43 proteinopathies) 45 and 25 kDa bands and high molecular weight smear in the TDP-43-positive PSP case. These findings suggest that (1) although PSP is nominally a tauopathy, pathological TDP-43 can accumulate in the limbic system in some cases, and (2) TDP-43 pathology may be concurrent with HS.

O. Yokota · Y. Davidson · D. M. A. Mann (✉)
Neurodegeneration and Mental Health Research Group, Faculty of Medical and Human Sciences, School of Community Based Medicine, Greater Manchester Neurosciences Centre, Hope Hospital, University of Manchester, Salford M6 8HD, UK
e-mail: david.mann@manchester.ac.uk

S. Sikkink · S. Pickering-Brown
Neurodegeneration and Mental Health Research Group, Faculty of Medical and Human Sciences, School of Community Based Medicine, A V Hill Building, University of Manchester, Oxford Rd, Manchester M13 9PL, UK

E. H. Bigio
Department of Pathology, Northwestern University Feinberg School of Medicine, Chicago, IL 60619, USA

O. Yokota · H. Ishizu · S. Terada
Department of Neuropsychiatry, Okayama University Graduate School of Medicine, Dentistry and Pharmaceutical Sciences, 2-5-1 Shikata-cho, Okayama 700-8558, Japan

H. Ishizu
Zikei Institute of Psychiatry, 100-2, Urayasu-honcho, Okayama 702-8508, Japan

T. Arai · H. Akiyama
Department of Psychogeriatrics, Tokyo Institute of Psychiatry, 2-1-8 Kamikitazawa, Setagaya-ku, Tokyo 156-8585, Japan

M. Hasegawa
Department of Molecular Neurobiology, Tokyo Institute of Psychiatry, 2-1-8 Kamikitazawa, Setagaya-ku, Tokyo 156-8585, Japan

Keywords Argyrophilic grains · Hippocampal sclerosis · Progressive supranuclear palsy · Tau · TDP-43

Introduction

Transactivation-responsive DNA-binding protein of M_r 43 kDa (TDP-43) is a nuclear protein involved in transcriptional repression and alternative splicing. It was originally identified as a major component of ubiquitin-positive and tau-negative inclusions in the frontotemporal cortex and motor neurons in frontotemporal lobar degeneration (FTLD-U), with or without progranulin gene mutations, and in amyotrophic lateral sclerosis (ALS) [3, 12, 31]. Subsequent studies revealed that TDP-43 is also abnormally accumulated in familial FTLD-U with mutations in the valosin-containing protein gene [32], in familial FTLD with motor neuron disease linked to chromosome 9p [10], and in ALS with TDP-43 gene mutations [25, 38, 41, 44]. TDP-43 is considered to play an essential pathogenic role in these diseases, now-called TDP-43 proteinopathies.

Although TDP-43 accumulation was originally considered to be a specific disease marker for FTLD-U and ALS, subsequent studies demonstrated that abnormal TDP-43 accumulation in some cases of other neurodegenerative diseases, such as Alzheimer's disease (AD) [2], Parkinson's disease with and without dementia [30], dementia with Lewy bodies (DLB) + AD [4, 30], ALS/parkinson-dementia complex of Guam (ALS/PDC of Guam) [15, 16], argyrophilic grain disease (AGD) [14], and Huntington disease [37]. However, the pathophysiological significance of concurrent TDP-43 accumulation, and its impact on clinical phenotype in these diseases remain unclear.

Several previous studies have suggested that cases of progressive supranuclear palsy (PSP) lack abnormal TDP-43 accumulation [3, 18, 40]. In these early studies, phosphorylation-independent antibodies were employed in TDP-43 immunohistochemistry and immunoblot analysis. We have made polyclonal and monoclonal antibodies specific for phophorylated TDP-43, which identify phosphorylation sites in the C-terminus of the TDP-43 accumulated in FTLD-TDP brains [17, 20], and selectively immunolabel pathological inclusions and dystrophic neurites without physiological nuclear staining in FTLD-TDP, ALS, AD with TDP-43 pathology, and in DLB with TDP-43 [4, 17]. They also recognize hyperphosphorylated TDP-43 at 45 kDa and additional 18–26 kDa fragments in sarkosyl-insoluble fractions on immunoblotting.

The principal aim of this study was to revisit the presence or absence, and the frequency, of TDP-43 pathology in PSP cases using a phosphorylation-dependent anti-TDP-43 antibody. In contrast to previous reports, we demonstrated that a significant proportion of PSP cases had variable degrees of TDP-43 pathology in the limbic system. We subsequently examined the relationships between TDP-43 pathology, tau pathology, and hippocampal sclerosis, as well as biochemical nature of the abnormally accumulated TDP-43, in PSP.

Materials and methods

Subjects

We investigated 19 pathologically confirmed PSP cases, 12 pathologically confirmed corticobasal degeneration (CBD) cases and 4 pathologically normal control subjects (Table 1). These cases were obtained from UK Parkinson's Disease Society Tissue Bank (7 PSP and 4 control cases), Department of Pathology, Northwestern University Feinberg School of Medicine Cognitive Neurology and Alzheimer Disease Center (5 PSP and 7 CBD cases), and Department of Neuropsychiatry, Okayama University Graduate School of Medicine, Dentistry and Pharmaceutical Sciences (7 PSP and 5 CBD cases). All brains had been collected with Local Research Ethical Committee approval. All PSP cases showed characteristic tufted astrocytes, and all CBD cases astrocytic plaques, as revealed by Gallyas-Braak silver methods and tau immunohistochemistry.

Immunohistochemistry

Sections cut at 5-μm thickness to include the amygdala, entorhinal cortex, hippocampus, occipitotemporal cortex in all cases, as well as the substantia nigra in two cases for which tissue was available, were stained with antibodies against phosphorylated TDP-43 (pAb pS409/410, rabbit, polyclonal, 1:1,000 [17]), phosphorylated tau (AT8, mouse, monoclonal, 1:3,000, Innogenetics, Ghent, Belgium), phosphorylated α-synuclein (#1175, rabbit, polyclonal, 1:1,000, [33]), and Aβ (4G8, mouse, monoclonal, 1:2,000, Covance Research Products Inc., Dedham, MA, USA). Deparaffinized sections were incubated with 1% H_2O_2 in methanol for 20 min to eliminate endogenous peroxidase activity in the tissue. When using anti-α-synuclein and anti-TDP-43 antibodies, sections were pretreated to enhance immunoreactivity in a microwave oven for 5 min in 10 mM sodium citrate buffer, pH 6.0, at 100°C. After blocking with 10% normal serum, sections were incubated 1 h at room temperature with the primary antibody. After three 5-min washes in phosphate-buffered saline (PBS), sections were incubated in biotinylated secondary antibody for 30 min, and then in avidin-biotinylated horseradish peroxidase complex (ABC Elite kit, Vector, Burlingame, CA, USA) for

Table 1 Demographic data in PSP and CBD cases with and without TDP-43 pathologies

	PSP			CBD		
	All	TDP-43-positive PSP	TDP-43-negative PSP	All	TDP-43-positive CBD	TDP-43-negative CBD
N (%)	19	5 (26.3)	14 (73.7)	12	2 (16.7)	10 (83.3)
Male [*N* (%)]	16 (84.2)	4 (80.0)	12 (85.7)	7 (58.3)	1 (50.0)	6 (60.0)
Age at onset [mean (SD)]	68.3 (9.8)	75.0 (9.4)	65.7 (9.0)	55.2 (10.2)	49.0 (12.7)	56.6 (9.9)
Age at death [mean (SD)]	76.3 (10.7)	82.4 (11.7)	74.1 (9.8)	62.8 (11.2)	56.0 (15.6)	64.1 (10.7)
Duration [mean (SD)]	7.4 (4.4)	7.4 (4.6)	7.5 (4.6)	7.3 (2.9)	7.0 (2.8)	7.3 (3.1)
Dementia (%)	11 (57.9)	4 (80.0)	7 (50.0)	11 (91.7)	2 (100.0)	9 (90.0)
Brain weight [g, mean (SD)]	1,202 (142)	1,234 (180)	1,190 (132)	1,174 (146)	1,008 (152)	1,215 (120)
Argyrophilic grains [*N* (%)]	4 (21.1)	1 (20.0)	3 (21.4)	3 (25.0)	1 (50.0)	2 (20.0)
Hippocampal sclerosis [*N* (%)]	3 (15.8)	3 (60.0)	0 (0.0)	0 (0.0)	0 (0.0)	0 (0.0)

30 min. The peroxidase labeling was visualized with 0.2% 3,3′-diaminobenzidine (DAB) as chromogen. Sections were lightly counterstained with hematoxylin.

Semiquantitative assessment

TDP-43, tau, and Aβ pathologies in the amygdala, anterior and posterior portions of the entorhinal cortex, hippocampal dentate gyrus, CA1, 2, 3, and 4 regions, subiculum, fusiform gyrus, occipitotemporal gyrus were semiquantitatively evaluated using the following grading system blinded to any clinical or pathological information:

1. The total number of TDP-43-positive neuronal cytoplasmic inclusions (NCIs) in each anatomical region was assessed as follows: − no lesion, + one inclusion, ++ two or three inclusions, +++ four or five inclusions, ++++ 6–10 inclusions, +++++ 11 or over inclusions. In addition, the presence or absence of neuronal intranuclear inclusions (NIIs) and dystrophic neurites was also assessed. Then, we classified the topographic distribution of TDP-43 pathological changes using following system, which is similar to that reported by Amador-Ortiz et al. [2]: the amygdala type: inclusions were present only in the amygdala; the limbic type: inclusions extend to the amygdala, hippocampal dentate gyrus, CA1-4, entorhinal cortex, and fusiform gyrus, but not in the occipitotemporal gyrus; the temporal type: inclusions are present in the limbic system and also the in the occipitotemporal gyrus.
2. Tau-positive neuronal inclusions were counted in low power microscopic fields: 0, no tau-positive lesions; 1, one neuronal inclusion per few microscopic fields; 2, one inclusion in every field; 3, 4–30 inclusions in every field; 4, over 30 inclusions associated with numerous neurites in every field.
3. Aβ deposits were counted in low power microscopic fields: 0, no Aβ deposits; 1, two to three Aβ plaques in each field; 2, 4–10 Aβ plaques in each field; 3, 11–20 Aβ plaques in each field; 4, more than 20 Aβ deposits in each field.

Hippocampal sclerosis (HS) was defined by neuronal loss with gliosis in the hippocampal CA1 and/or subiculum, with relatively preserved neurons in the CA4, 3, and two regions and absence of intracellular and extracellular NFTs, or ischaemic changes that might explain neuronal loss in the CA1 and subiculum. HS was assessed blind to any clinical or pathological information.

Statistical analysis

The Mann–Whitney *U* test and Fisher's exact test were used to compare the demographic and pathological data between TDP-43-positive and TDP-43-negative groups in PSP and CBD series, respectively. Correlations between ratings of TDP-43 pathology and demographic data, or ratings of tau and Aβ pathologies in each anatomical region were assessed with Spearman's rank-order correlation statistic. Statistical analysis was performed using StatView for Macintosh program, version J-4.5. A value of $p < 0.05$ was accepted as significant.

Confocal laser scanning microscopy

Double-labeling immunofluorescence was performed with the combination of phosphorylation-dependent anti-TDP-43 (pAb pS409/410, rabbit, polyclonal, 1:1,000 [17]) and anti-tau antibodies (AT8, mouse, monoclonal, 1:500, Innogenetics, Ghent, Belgium). Sections from the amygdala and hippocampus in some PSP cases with TDP-43 pathology were pretreated by heating in a microwave oven for 5 min in 10 mM sodium citrate buffer, pH 6.0, at

100°C, allowed to cool then permeabilized with 0.2% (v/v) Triton X-100 in PBS. Following washing in PBS, non-specific antibody binding was blocked with normal sera and sections were incubated with a mixture of the two primary antibodies for 1 h at room temperature. After washing in PBS, sections were incubated with fluorescence-labeled secondary antibodies [AlexaFluor 488 anti-rabbit IgG (1:200) and AlexaFluor 555 anti-mouse IgG (1:200), Molecular Probes, Invitrogen, Paisley. UK]. After washing with PBS, sections were incubated with Toto-3 Iodide (Molecular Probes, Invitrogen, Paisley, UK) with 1 mg/ml RNase (Roche Diagnostics GmbH, Manheim, Germany) at 37°C. To quench (lipofuscin) autofluorescence, sections were incubated in 0.1% Sudan Black B for 10 min at room temperature and washed with 0.1% Tx-PBS for 30 min. Sections were coverslipped with Vectashield mounting media (Vector Laboratories Inc., Burlingame, CA, USA). Images were collected on a Leica TCS SP5 AOBS upright confocal (Leica Microsystems, Milton Keynes, UK) using the 488 nm (19%), 543 nm (30%) and 633 nm (60%) laser lines, respectively. To eliminate cross-talk between channels, the images were collected sequentially.

Immunoblotting

Frozen tissue from the amygdala, hippocampus, and frontal, temporal, and occipital cortices in one PSP case with TDP-43 pathology, one FTLD-TDP case (as a positive control) and eight negative controls (six PSP, one LBD, and one pathologically normal case) were prepared for western blotting according to methods previously described by Neumann et al. [31]. Briefly, 1 g of fresh frozen brain was homogenized in 5 ml/g (w/v) of low salt (LS) buffer-containing 10 mM Tris pH 7.5, 5 mM EDTA pH 8.0, 1 mM DTT, 10% (w/v) sucrose and Roche complete EDTA-free protease inhibitor. Homogenates were sequentially extracted with increasing strength buffers [Triton X-100 buffer (LS buffer + 1% Triton X-100 + 0.5 M NaCl), Triton X-100 buffer with 30% sucrose to float myelin, Sarkosyl buffer (LS buffer + 1% *N*-lauroyl-sarcosine + 0.5 M NaCl)]. Detergent-insoluble pellets were extracted in 0.25 ml/g Urea buffer (7 M Urea, 2 M Thiourea, 4% 3-[(3-Cholamidopropyl) dimethylammonio]-1-propanesulfonate (CHAPS), 30 mM Tris–HCl pH 8.5, Roche complete EDTA free protease inhibitor. Prior to SDS-PAGE immunoblot analysis, urea fractions were added in 1:1 ratio to SDS sample buffer (10 mM Tris pH 6.8, 1 mM EDTA, pH 8.0, 40 mM DTT, 1% SDS, 10% Sucrose, 0.01% Bromophenol Blue). Protein was resolved on 12% Tris–Glycine SDS-PAGE gels along with size standard (Bio-Rad kaleidoscope broad-range marker; Bio-Rad, Hercules, CA, USA). Proteins were transferred onto nitrocellulose membrane (Hybond ECL, GE Life Sciences, UK) and blocked for 1 h at 4°C in 5% (w/v) milk solution [5% powdered milk in Tris-buffered saline containing 0.1% Tween-20 (TBS-T)]. Membranes were incubated in phosphorylation-dependent mouse monoclonal antibody (mAb pS409/410, mouse, 1:1,000 [20]) for 1 h at room temperature followed by HRP-conjugated goat anti-mouse secondary antibody (Santa Cruz Biotechnology Inc, CA, USA). Antibodies were visualized by incubating in enhanced chemiluminescent reagent (ECL, GE Life Sciences) and imaged using the ImageQuant 350 system fitted with a F0,95 25 mm Fixed Lens (GE Healthcare, Life Sciences, UK). TDP-43 probed membranes were exposed for 5 min at different timeframes to obtain multiple images of differing intensity. Images were processed using ImageQuant TL software (GE Healthcare, Life Sciences, UK).

Results

Frequency and distribution of TDP-43 pathology

Clinical and pathological features for all subjects are shown in Table 1. TDP-43 pathology was noted in 5 of 19 PSP cases (26%) and in 2 of 12 CBD cases (17%). Disease duration, gender ratio and brain weight were not statistically different between PSP cases with and without TDP-43 pathology, or between CBD cases with and without TDP-43 pathology, respectively. Age at onset of disease (75 vs. 66 years) and age at death (82 vs. 74 years) tended to be higher, and dementia occurred more often, in PSP cases with TDP-43 pathology than in PSP cases without it (80 vs. 50%), although these differences did not reach statistical significance. One PSP case without TDP-43 pathology also had Lewy body pathology corresponding to brainstem-predominant type [26]. Ten PSP cases (3 TDP-43-positive and 7 TDP-43-negative cases) and four CBD cases (all were TDP-43-negative) had Aβ-positive diffuse plaques in the amygdala, hippocampus, and/or temporal cortex. Of the three TDP-43-positive PSP cases, one case had only a few neuritic plaques in the occipitotemporal gyrus. None of the PSP or CBD cases in our series fit the pathological criteria of AD [9, 28, 39].

In PSP cases, TDP-43-positive NCIs were most frequently noted in the amygdala and dentate gyrus granule cells in the hippocampus (5 cases, 100% of TDP-43-positive PSP cases), followed by the anterior portion of the entorhinal cortex (4 cases, 80%), subiculum (3 cases, 60%), posterior portion of the entorhinal cortex (3 cases, 60%), occipitotemporal gyrus (2 cases, 50%), fusiform gyrus (2 cases, 40%), and CA1 region (2 cases, 20%) (Table 2, Fig. 1a–d). In addition to the rounded inclusions noted in FTLD-TDP, all PSP cases had many irregular shaped

Table 2 Distribution of TDP-43 pathology in PSP and CBD cases

TDP-43 pathology												Hippocampal sclerosis (CA1/Subiculum)	Argyrophilic grains[b]
No.	Amygdala	ant.EC	DG	CA3/4	CA2	CA1	SB	post.EC	FG	OTG	TDP-43 distribution[a]		
PSP cases													
PSP1	++++	−	+	−	−	−	−	−	−	−	Limbic	−	−
PSP2	+++++	+++++	+++++	−	−	−	+	−	−	n	Limbic	+	−
PSP3	+++++	+++++	+++	−	−	−	++	++++	−	−	Limbic	−	−
PSP4	+++++	+++++	++	−	−	+	+++	+++++	+++++	+	Temporal	+	−
PSP5	+++++	+++	+++++	−	−	++	−	++	+++	+++	Temporal	+	Stage III
%	100.0	80.0	100.0	0.0	0.0	20.0	60.0	60.0	40.0	50.0		60.0	20.0
CBD cases													
CBD1	+++	++	−	−	−	−	−	n.a.	n.a.	n.a.	Limbic	−	−
CBD2	+++++	++	++++	++	−	+++++	+++++	++	−	−	Limbic	−	Stage II
%	100.0	100.0	50.0	50.0	0.0	50.0	50.0	50.0	0.0	0.0		0.0	50.0

The stages of TDP-43 pathology: −, no lesion in the anatomical region; +, 1 inclusion in the anatomical region; ++, 2–3 inclusions in the anatomical region; +++, 4–5 inclusion in the anatomical region; ++++, 6–10 inclusions in the anatomical region; +++++, 11 or over inclusions in the anatomical region. The stage of hippocampal sclerosis: −, no; +, mild; ++, moderate; +++, severe. The stage of argyrophilic grains: −, absent; +, present. ant.EC, the anterior portion of the entorhinal cortex; DG, hippocampal dentate gyrus; SB, subiculum; post.EC, the posterior portion of the entorhinal cortex; FG, fusiform gyrus; OTG, occipitotemporal gyrus

[a] The amygdala type: inclusions were present only in the amygdala; the limbic type: inclusions extend to the limbic system, but not in the occipitotemporal gyrus; the temporal type: inclusions are present in the limbic system and occipitotemporal gyrus as well

[b] The distribution of argyrophilic grains are assessed using a staging system proposed by Saito et al. [35]

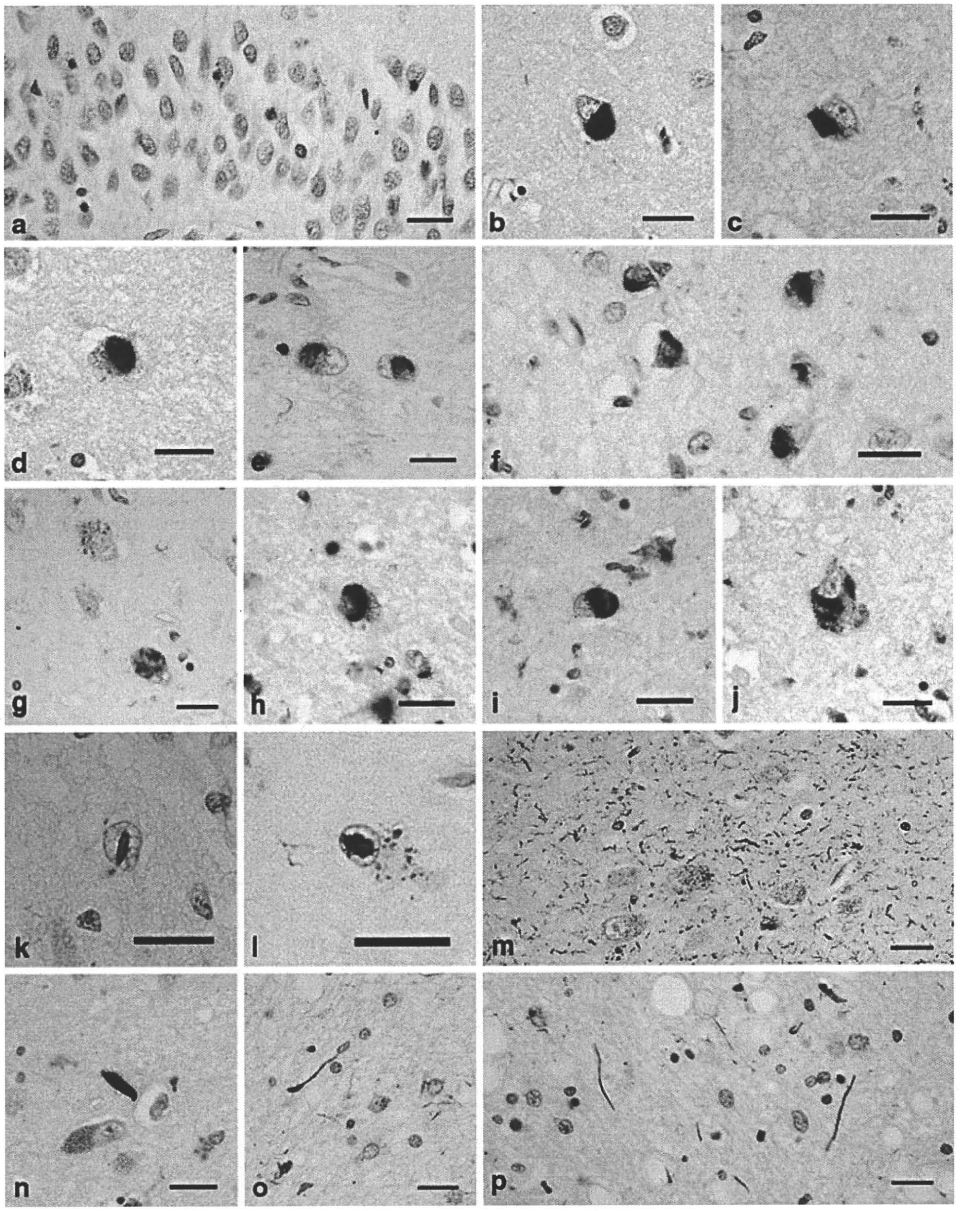

Fig. 1 TDP-43-positive lesions in PSP. **a** Neuronal cytoplasmic inclusions (NCIs) in the hippocampal dentate gyrus. **b–d** NCIs in the entorhinal cortex. Irregular shaped NCIs in the entorhinal cortex (**e**), fusiform gyrus (**f**), and subiculum (**g**). These inclusions have weakly stained or unstained regions. Small dot-like structures are also seen in the neuronal cytoplasm (**g**). Horseshoe-shaped (**h**, **i**) and NFT-like (**j**) NCIs in the entorhinal cortex. Intranuclear inclusions in the amygdala (**k**) and in the subiculum (**l**), cases PSP3 and PSP2, respectively. **m** Massive short threads-like structures in the subiculum, case PSP3. **n** Thick, thread-like structures in the amygdala. **o**, **p** Long, thin thread-like structures in the amygdala. pAb pS409/410 immunohistochemistry. All *scale bars* 20 μm

NCIs, such as flame-shape NFT-like, globose-type NFT-like, and horseshoe-like inclusions (Fig. 1e–j). One PSP case (PSP 2 in Table 2) showed a few NII in the subiculum (Fig. 1k, l). Two cases (PSP4 and PSP5) had abundant fine, short, thread-like structures immunopositive for TDP-43 from the CA1 to subiculum (Fig. 1m). TDP-43-positive thread-like structures were also observed in the amygdala (3 cases), entorhinal cortex (2 cases), CA1 (one case), and subiculum (one case) (Fig. 1n–p).

In two CBD cases, TDP-43-positive NCIs were observed in the amygdala, entorhinal cortex, hippocampal dentate gyrus, CA1, CA3/4, and subiculum (Table 2, Fig. 2a). The distribution of TDP-43 pathology was roughly consistent with that observed in PSP cases. NIIs were found in the subiculum and amygdala in one CBD case with severe TDP-43 pathology (Fig. 2b, c). Short thread-like structures immunopositive for TDP-43 were found in the amygdala, entorhinal cortex, CA1, CA3, and/or subiculum in both CBD cases with TDP-43 pathology. One CBD case had TDP-43-positive coiled body-like structures and thread-like structures in the alveus in the subiculum (Fig. 2d–f). Abnormal accumulation of TDP-43 was not found in the white matter of the temporal lobe and substantia nigra in any of the TDP-43-positive PSP or CBD cases.

Relationship between TDP-43 pathology and tau or Aβ burden

The ratings for tau burden in the TDP-43-positive PSP cases tended to be higher (but not significantly so) than

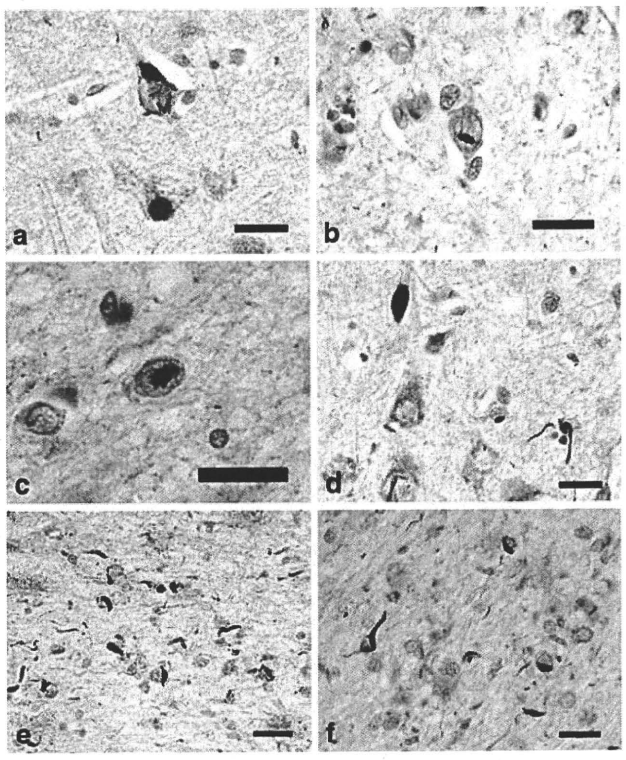

Fig. 2 TDP-43-positive lesions in CBD. **a** Neuronal cytoplasmic inclusions (NCIs) in CA3 region of hippocampus. **b**, **c** Neuronal intranuclear inclusions in the amygdala. **d** A thick neurite and thin, thread-like structures in the amygdala. **e** Short thread-like structures and glial cytoplasmic inclusions (GCIs) in the alveus in the entorhinal cortex. **f** Coiled body-like structures and GCis in the alveus in the entorhinal cortex. pAb pS409/410 immunohistochemistry. All *scale bars* 20 μm

those in the TDP-43-negative PSP cases, in almost all regions examined (i.e., including amygdala, entorhinal cortex, hippocampal dentate gyrus, CA1-4, fusiform gyrus, and occipitotemporal gyrus) (Fig. 3). In the PSP cases overall, rating for tau pathology in the occipitotemporal gyrus was significantly correlated with that of TDP-43 pathology ($r = 0.504$, $p < 0.05$), but no significant correlations between tau and TDP-43 ratings were found in any other regions. There were no significant differences in the degree of Aβ burden in any region between TDP-43-positive and TDP-43-negative PSP cases, and ratings for TDP-43 pathology did not correlate with those for Aβ burden in any region. Of three TDP-43-positive PSP cases having Aβ deposits, only one case had a few neuritic plaques in the occipitotemporal gyrus; however, this case did not have any TDP-43-positive inclusions in the region.

In the CBD cases, there were no significant differences in tau or Aβ burden in any region between TDP-43-positive and TDP-43-negative cases, and ratings for TDP-43 pathology did not correlate with those for tau or Aβ burden in any region.

Relationship of HS, argyrophilic grains, TDP-43 accumulation, and dementia

In 3 of 19 PSP cases (16%), evident neuronal loss in the CA1 and subiculum consistent with HS was noted (Fig. 4a, b). No CBD case showed HS. All three PSP cases with HS had a various degrees of TDP-43 pathology in the CA1 and/or subiculum (Fig. 4e–h), and two had extensive TDP-43

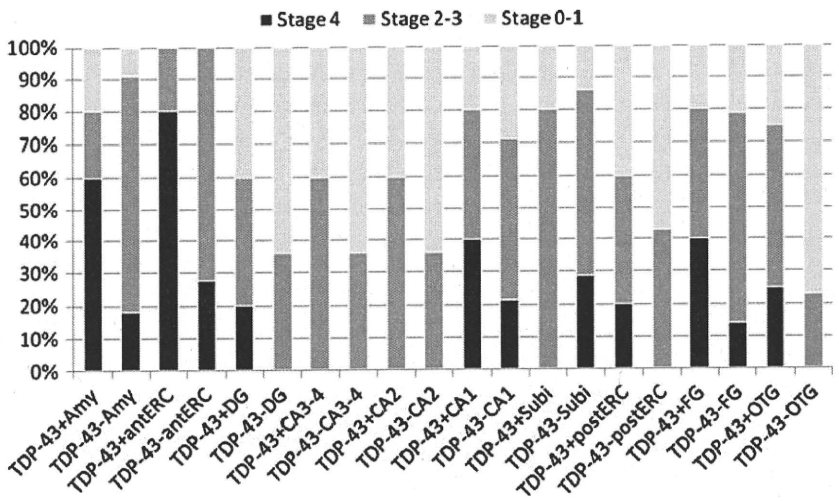

Fig. 3 Tau burden in the limbic system in PSP cases with and without TDP-43 pathology. In all regions but the subiculum, tau burden in PSP cases with TDP-43 pathology is more severe than that in PSP cases without TDP-43 pathology. Stage 0–1, no to mild tau deposition; stages 2–3, moderate to severe tau deposition; stage 4, very severe tau deposition (see detailed definition in the text). *TDP-43+* TDP-43-positive, *TDP-43−* TDP-43-negative, *Amy* amygdala, *antERC* the anterior portion of the entorhinal cortex, *DG* hippocampal dentate gyrus, *Subi* subiculum, *postERC* the posterior portion of the entorhinal cortex, *FG* fusiform gyrus, *OTG* occipitotemporal gyrus

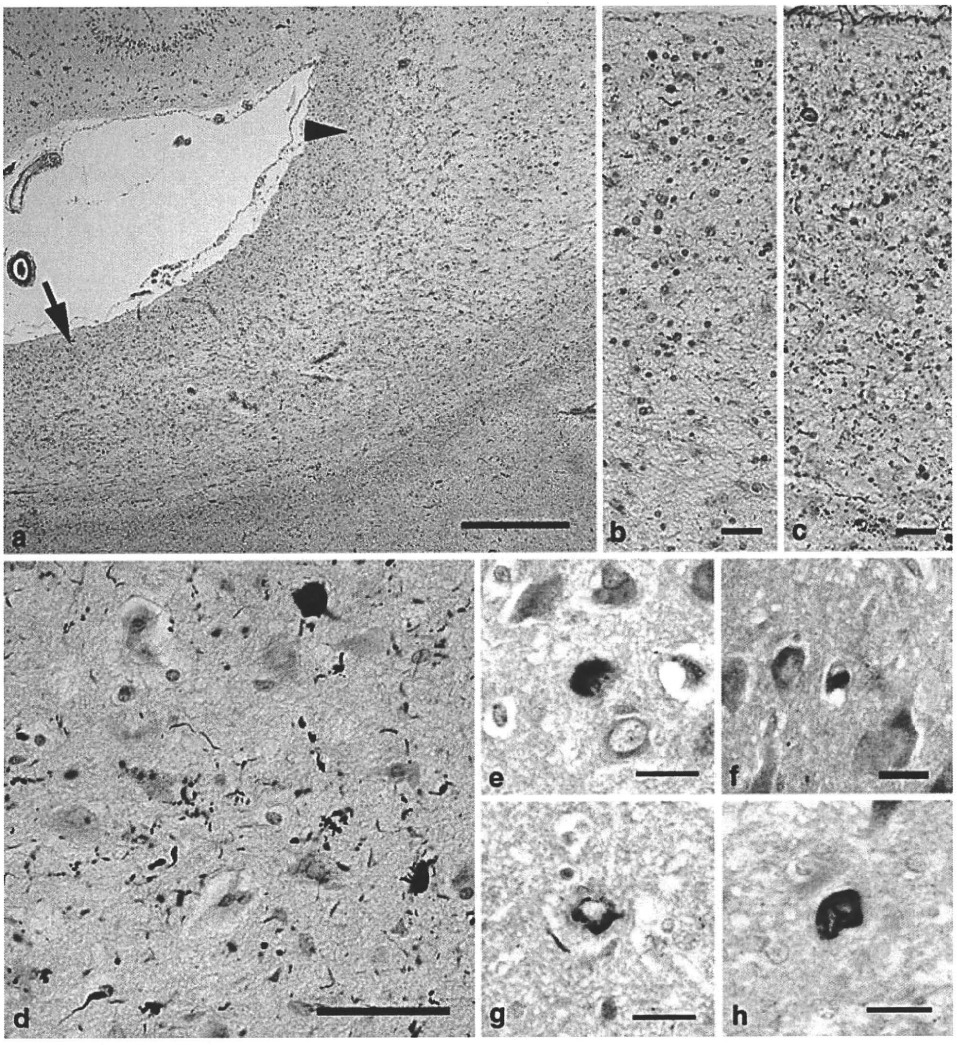

Fig. 4 Pathological features in the hippocampus in a PSP case with TDP-43, HS, and argyrophilic grains (PSP5). **a** A low power view of the hippocampal CA1 to subiculum. Severe reduction of the width with tissue rarefaction is noted in the subiculum (*arrow*) and to a lesser degree in the adjacent CA1 region (*arrowhead*). **b** A moderate power view of the subiculum on the same section as that shown in **a**. Severe neuronal loss associated with gliosis is evident. Argyrophilic threads and grains are scattered, but tangles are rare. **c** The subiculum on an adjacent section of **b**. A moderate number of tau-positive threads and grains, but only a few tangles, are seen. **d** Argyrophilic grains in CA1 region. **e**, **f** TDP-43-positive cytoplasmic inclusions in CA1 region. **g** An irregular shaped TDP-43 accumulation in the subiculum. **h** A coiled body-like TDP-43-positive inclusion in the subiculum. **a**, **b**, **d** Gallyas-Braak hematoxylin-eosin stain. **c** AT-8 immunohistochemistry. **e–h** pAb pS409/410 immunohistochemistry. *Scale bars* **a** 400 μm, **b**, **c** 25 μm, **d** 50 μm, **e–h** 20 μm

pathology in the limbic system: one case had both TDP-43 pathology and argyrophilic grains (Table 2). Two of the three PSP cases with HS had a few AT8-positive pretangles and argyrophilic grains in the CA1 and subiculum (Fig. 4b–d). Neurofibrillary tangles were rare in these regions in all PSP cases with HS (Fig. 4b). No significant ischemic changes in the hippocampal pyramidal neurons, or neuronal loss in the end plate, suggestive of a past history of severe epilepsy was noted in any of the PSP cases with HS. The frequency of HS in the TDP-43-positive PSP cases was significantly higher than that in TDP-43-negative PSP cases (60 vs. 0%, $p = 0.021$). Dementia was present in all of the 3 TDP-43-positive PSP cases with HS (100%), 4 of the 5 TDP-43-positive PSP cases with and without HS (80%), 1 of 2 TDP-43-positive PSP cases without HS (50%), and 7 of 14 PSP cases lacking both (50%). The frequency of dementia was not significantly different between PSP cases with and without HS ($p = 0.170$).

Concomitant argyrophilic grains were observed in four PSP (21%) and three CBD cases (25%) (Fig. 4d). Among these cases, one PSP and one CBD case had TDP-43 pathology (Table 2, Fig. 4e–h). There was no significant difference in the frequency of argyrophilic grains between TDP-43-positive and TDP-43-negative PSP cases, or between CBD cases with and without TDP-43 pathology, respectively. However, in the TDP-43-positive PSP and CBD cases, argyrophilic grains were found in those cases with the most severe TDP-43 pathology (Table 2).

Double immunofluorescence labeling in PSP cases

In the PSP cases examined, TDP-43 and tau pathologies were independently present in the perikarya of granular cells in the hippocampal dentate gyrus with no coexistence of these proteins (Fig. 5a–f). In contrast, in the amygdala, TDP-43 accumulation was often intermingled with tau accumulation in NCIs and dystrophic neurites, and colocalization was frequent (Fig. 5g–o). In the entorhinal cortex and parahippocampal gyrus in one PSP case with argyrophilic grains, many tau-positive grain-like structures

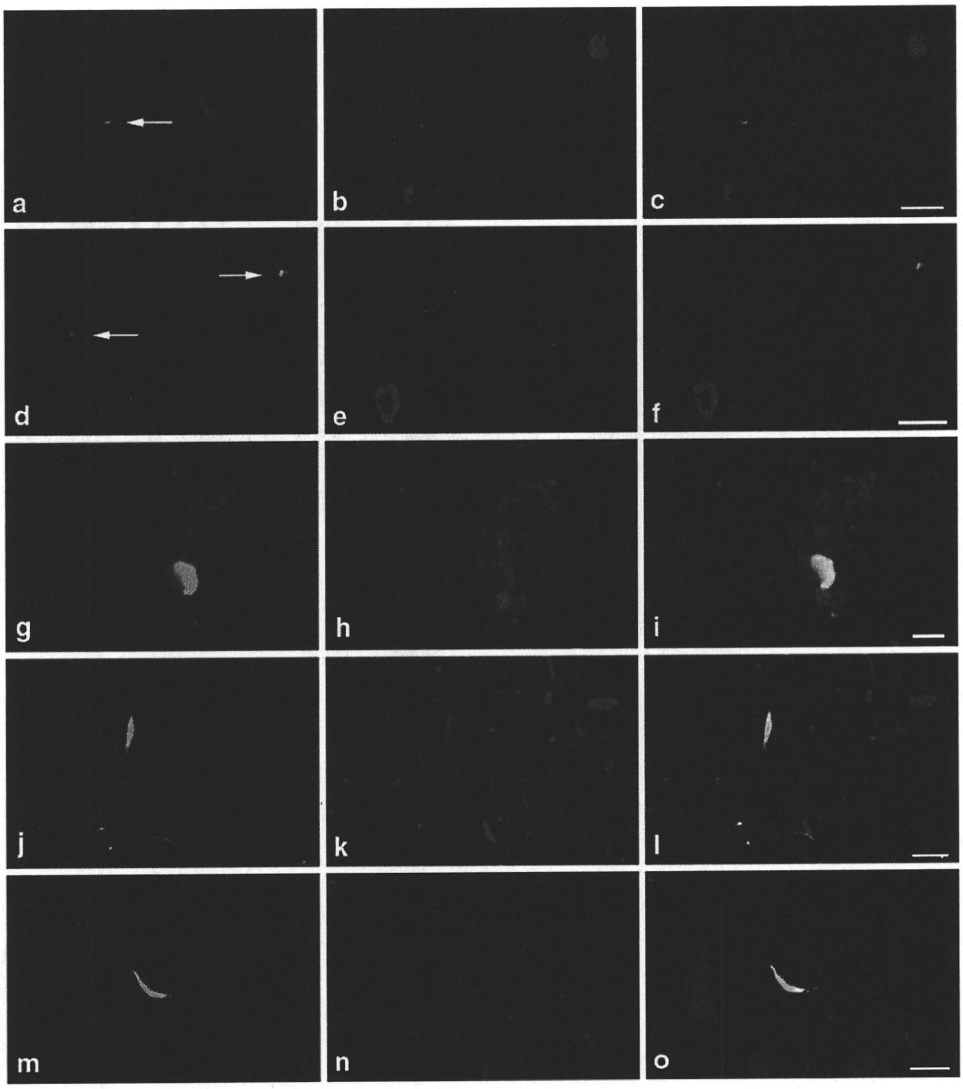

Fig. 5 Confocal double-imunofluorescence of TDP-43 (**a**, **d**, **g**, **j**, **m**) and tau (**b**, **e**, **h**, **k**, **n**) in PSP cases. *Merged images* are shown in **c**, **f**, **i**, **l**, and **o**. Blue fluorescence in merged images are nuclei. **a–f** In the hippocampal dentate gyrus, TDP-43 accumulation (*arrows*) is not colocalized with tau labeling. **g–i** In the amygdala, TDP-43 accumulation is often intermingled and colocalized with neuronal tau accumulation. **j–o** TDP-43-positive neurites (**j**, **m**) and many tau-positive neurites and granules (**k**, **n**) are seen in the amygdala. Coexistence of TDP-43 and tau is noted in some neurites (**l**, **o**). AT8 and pAb pS409/410 double immunofluorescence. *Scale bars* **a–c** 25 μm, **d–f** 25 μm, **g–i** 2.5 μm, **j–l** 7.5 μm, **m–o** 7.5 μm

were demonstrated, and TDP-43 was colocalized with tau in some of these structures (data not shown).

Biochemical analyses of TDP-43 in PSP cases

Immunoblot analysis of the sarkosyl-insoluble, urea-soluble fraction with mAb pS409/410 demonstrated distinct bands at (approximately) 45 and 25 kDa, as well as high molecular weight smears in the amygdala of a PSP case having TDP-43 pathology (Fig. 6, lane 6) and in the frontal cortex of a FTLD-TDP case (lane 5). Weak 25 and 45 kDa bands were also observed in the hippocampus in a PSP case, which had very mild TDP-43 pathology at this site (lane 7). Pathological TDP-43 bands and smear were not demonstrated in any of the other cases lacking TDP-43 pathology, including those with PSP (lanes 1 and 2) or Lewy body disease (lane 4), or in normal control cases (lane 3).

Discussion

This is the first study demonstrating abnormal accumulations of phosphorylated TDP-43 in the limbic system in a significant proportion (26%) of patients with PSP. Immunoblot analysis also demonstrated biochemical alterations in TDP-43 in tissue samples from a PSP case with TDP-43 pathology, similar to those in FTLD-TDP and ALS. Regional tau burden in PSP cases with TDP-43 pathology was higher than that in PSP cases without it, and TDP-43 burden was significantly correlated with that of tau in the occipitotemporal cortex. The frequency of HS in PSP cases with TDP-43 pathology was significantly higher than that in PSP cases without it. Collectively, these findings suggest that (1) PSP is one of the tauopathies in which pathological TDP-43 accumulation can occur in the limbic system, and (2) TDP-43 pathology may be associated with the occurrence of HS in PSP cases.

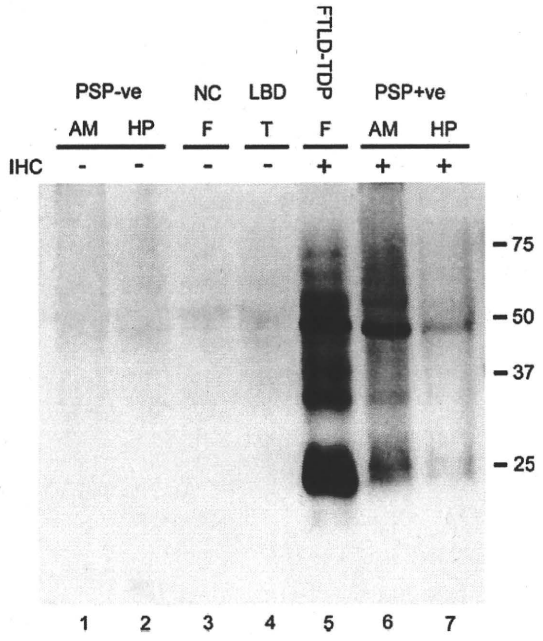

Fig. 6 Immunoblot analysis of the sarkosyl-insoluble fraction in representative PSP cases with phosphorylation-dependent monoclonal anti-TDP-43 antibody (mAb pS409/410). The 45 kDa full length TDP-43, 25 kDa fragments, and high molecular weight smear are strongly labeled in the amygdala of a PSP case with TDP-43 pathology (*lane 6*) and in the frontal cortex of a FTLD-TDP case (*lane 5*). Weakly stained 45 and 25 kDa bands are noted in the hippocampus of a PSP case (*lane 7*), in which TDP-43 pathology was mild. Similar 45 and 25 kDa bands and smears were not immunolabeled in any of the other cases without detectable TDP-43 pathology by immunohistochemistry (*lanes 1–4*). Normal 43 kDa TDP-43 is not stained by this phophorylation-dependent antibody in any case. *PSP* progressive supranuclear palsy, *LBD* Lewy body disease, *NC* normal control, *AM* amygdala, *HP* hippocampus, *F* frontal cortex, *T* temporal cortex, *IHC* pAb pS409/410 immunohistochemistry

Previous studies have demonstrated variable frequencies of concurrent TDP-43 pathology in many tauopathies: 23–56% in AD cases [2, 4, 40], 31–60% in DLB + AD cases [4, 30], 15% in CBD cases [40], and 60% in AGD cases [14]. Why no cases of PSP with TDP-43 pathology have previously been described is not clear. Our present findings show that, at least some, PSP cases may share a common pathophysiological background involving TDP-43 accumulation with other tauopathies with TDP-43 pathology. Several studies demonstrated that concurrent AD-type pathology was associated with the development of TDP-43 pathology in some neurodegenerative diseases [2, 4, 7, 14, 30]. However, it was unlikely that the development of TDP-43 pathology in our PSP series can be explained by the influence of Aβ deposits or neuritic plaques. For example, of all ten PSP cases having Aβ deposits, nine cases had only diffuse plaques, and the degree of Aβ deposition was not significantly different between TDP-43-positive and TDP-43-negative PSP cases and was not correlated with that of TDP-43 pathology in any regions. Although only one PSP case had a few neuritic plaques in the occipitotemporal gyrus, no TDP-43-positive inclusion was noted in the region.

Our findings are inconsistent with previous studies that failed to demonstrate immunohistochemical or biochemical abnormalities of TDP-43 in PSP cases [2, 3, 18, 40]. Considering that the sample size investigated in one of these previous studies [40] was far larger than that in our own study, the most plausible cause of the discrepancy may be the difference of the sensitivities of anti-TDP-43 antibodies employed: phosphorylation-dependent anti-TDP-43 antibodies do not stain normal nuclei, making true TDP-43-positive inclusions more readily identifiable [17, 37]. The distribution of TDP-43 pathology observed in our PSP cases was very similar to that reported previously in AD [2, 4, 18, 19, 40], DLB + AD [4, 30], and CBD [40], but tended to be more restricted than that in ALS/PDC of Guam [15, 16, 27]. Most frequently affected sites in these tauopathies are the amygdala and hippocampal dentate gyrus. Given these findings, it is plausible that the frequent TDP-43 accumulation in these sites in tauopathies is associated with some region-specific, rather than disease-specific, mechanism. On the other hand, it remains unclear whether TDP-43 is abnormally accumulated through an identical pathophysiological mechanism in various anatomical regions. For example, it was reported that abnormal TDP-43 accumulation was significantly correlated with the severity of tau pathology in AD cases [4] and Lewy body disease including many DLB + AD cases [30]. This same statistical relationship was observed in our PSP cases. Furthermore, in our present studies, TDP-43 was often colocalized with tau in NCIs and dystrophic neurites in the amygdala, although there were also TDP-43-positive but tau-negative lesions in this site. A coexistence of TDP-43 and tau in the same neuron in the amygdala and temporal cortex was also reported in AD and DLB cases in previous studies [4, 18]. However, in contrast to the amygdala, a coexistence of TDP-43 and tau in the same neuron in the hippocampal dentate gyrus was not seen in our PSP cases. This trend regarding non-colocalization of these two proteins was also noticed in the dentate granular cells in AD [40] and AGD brains [14]. This suggests that the mechanism underlying the accumulation of TDP-43 is different at least between the amygdala and hippocampal dentate gyrus, or that there is some unknown factor that can influence the occurrence of both TDP-43 and tau pathologies. In addition, considering the potential relationship between tau and TDP-43 in PSP presented in this paper, whether TDP-43 pathology is also noted in several other regions that are often involved by tau-associated lesions (e.g., the frontal cortex and basal ganglia) needs to be investigated in the future studies.